

Estimation of cerebrovascular reactivity amplitude and lag using breath-holding fMRI and the global BOLD signal: Application in diabetes and hypertension

Journal of Cerebral Blood Flow & Metabolism
0(0) 1–17
© The Author(s) 2024
Article reuse guidelines:
sagepub.com/journals-permissions
DOI: 10.1177/0271678X241270420
journals.sagepub.com/home/jcbfm



Nuwan D Nanayakkara¹ , Liesel-Ann Meusel¹,
Nicole D Anderson^{1,2} and J Jean Chen^{1,3,4}

Abstract

In this work, we demonstrate a data-driven approach for estimating cerebrovascular reactivity (CVR) amplitude and lag from breathhold (BH) fMRI data alone. Our approach employs a frequency-domain approach that is independent of external recordings. CVR amplitude is estimated from the BOLD frequency spectrum and CVR lag is estimated from the Fourier phase using the global-mean BOLD signal as reference. Unlike referencing to external recordings, these lags are specific to the brain. We demonstrated our method in detecting regional CVR amplitude and lag differences across healthy (CTL), hypertensive (HT) and hypertension-plus-type-2-diabetes (HT + DM) groups of similar ages and sex ratios, with a total N of 49. We found CVR amplitude to be significantly higher in CTL compared to HT + DM, with minimal difference between CTL and HT. Also, voxelwise CVR lag estimated in the Fourier domain is a more sensitive marker of vascular dysfunction than CVR amplitude. CVR lag in HT is significantly shorter than in CTL, with minimal difference between CTL and HT + DM. Our results support the importance of joint CVR amplitude and lag assessments in clinical applications.

Keywords

Cerebrovascular reactivity (CVR), breath-holding, global mean signal, diabetes mellitus, hypertension, hemodynamic lag

Received 30 March 2024; Revised 3 July 2024; Accepted 8 July 2024

Introduction

When mapping cerebrovascular reactivity (CVR) mapping,^{1–3} inhalation-based (gas challenge) methods can involve elaborate set up. Breath-hold (BH) tasks involve minimal setup and have been suggested as a robust alternative to gas challenges.^{4–7} BH tasks have been well tolerated by participants of vulnerable groups^{8,9} and have been successfully applied in clinical studies.^{9–12} A typical BH task follows a protocol consisting of a block design with alternating periods of normal breathing and breath holding for a simple reproducible voluntary breathing modulation task.^{5,13,14} Nonetheless, well-known caveats of BH methods include the greater need for participant cooperation^{6,15} and the unavailability of expired gas measurements during the BH periods, especially as a given BH task pattern across multiple participants do not necessarily produce similar increases in CO₂ partial pressure values in the blood.⁶ To help address this source of uncertainty, some studies have

incorporated measurement of end-tidal carbon dioxide partial pressure (PETCO₂) using a mask or nasal cannula.^{4,14,16} A short BH period of 6 s can result in hypercapnia¹⁷ while the spatial extent of the significant BOLD response reaches a plateau at a BH length of around 20 s.¹⁸ Many studies have reported a BH length of

¹Rotman Research Institute, Baycrest Academy for Research and Education, Toronto, Canada

²Departments of Psychology and Psychiatry, University of Toronto, Toronto, Canada

³Department of Medical Biophysics, University of Toronto, Toronto, Canada

⁴Department of Biomedical Engineering, University of Toronto, Toronto, Canada

Corresponding author:

J Jean Chen, Rotman Research Institute, Baycrest Academy for Research and Education, 3560 Bathurst Street, Toronto, ON M6A 2E1, Canada.
Email: jchen@research.baycrest.org

15 s for successful estimation of CVR from BOLD data.^{5,11,19–21} With careful analysis, the performances of BH can be comparable to those involving gas manipulation techniques.^{15,22–24} However, at the CVR estimation step, uncertainties in participant compliance can present major data-analysis challenges, especially when PETCO₂ recordings are unavailable.

Model-driven approaches such as the general linear model (GLM) have been employed to estimate CVR from BOLD responses to a BH task, whereby the BH paradigm is modelled as a boxcar^{25,26} or ramp function convolved with a hemodynamic response function (HRF) to approximate linear BOLD signal increases.⁴ Additional temporal derivatives of the HRF are required to account for the longer delays in respiratory responses to appear in the BOLD signal.^{27,28} The GLM model-driven approaches use a single fixed time lag in HRF to fully describe the BOLD signal across the whole brain. However, different brain regions exhibit different temporal CVR dynamics, both in healthy participants and in patients.^{14,20,21,29,30} Previous studies incorporating cross-correlations to estimate optimal time lags of the BOLD response have demonstrated substantial response-time variations across the brain.^{20,21} The global BOLD time series (GMS) has also been used in some studies as a whole-brain reference for shifting the PETCO₂ regressor²⁰ through iterative GLM fitting to estimate voxelwise CVR lag.^{14,20,27,31,32} However, it is evident that GLM methods work best when PETCO₂ recordings are available as input, allowing both inter-participant variations in BH compliance and in respiratory physiology to be accounted for.^{4,5,27,33} Moreover, the canonical hemodynamic response function is derived using the BOLD response to neuronal activity and not CO₂.

We propose a data-driven approach for estimating the amplitude and timing of the BH BOLD response without modelling or correlation with other signals (e.g. PETCO₂). Our approach makes use of the Fourier representation of the spectrum of BOLD data, as it has been found that the BH CVR response can be successfully approximated as a sinusoidal signal by assuming the BH task is approximately symmetrical (equivalent BH and baseline periods), even if it is not.^{5,27} This sinusoidal approach was shown to outperform the use of an HRF-based regressor (the PETCO₂ trace convolved with the HRF³¹) prompting us to estimate CVR in the Fourier domain. Our data-driven Fourier-based approach does not require regressors but instead detects and accounts for deviations from task designs directly from the BOLD fMRI data. Importantly, using the phase information in the GMS, we also demonstrate the estimation of CVR lags. In this study, we used a typical BH task design similar to the studies mentioned earlier. We

demonstrate our method by assessing differences in CVR amplitude and lag among patients with hypertension (HT), hypertension-plus-type-2 diabetes (HT + DM), and age-matched controls (CTL).

Methods

Study participants

Older adults of ages 65–85 were recruited and placed in control (CTL), hypertension (HT), or hypertension-plus-type-2-diabetes (HT + DM) groups based on screening measures. The study was approved by the Baycrest Ethics Board, which grants ethical approval guided by the Canadian Tri-Council policy statement titled “Ethical Conduct for Research Involving Humans”, drafted in accordance with the Declaration of Helsinki. A written informed consent was obtained from all participants. Participants were excluded from the study if they met any of the following criteria: (1) a score ≤ 31 on the Telephone Interview for Cognitive Status – modified version³⁴ in order to exclude participants with possible dementia; (2) the use of insulin to treat DM; (3) the presence of DM complications, based on self-report, including clinically significant gastroparesis, retinopathy, nephropathy, neuropathy, hepatic disease, or a recent coronary heart disease event as determined by a physician; (4) other significant medical or psychiatric disorders affecting cognitive function, such as stroke and major depressive disorder; (5) current or recent use of central nervous system-active medications, including those for the treatment of depression, sleep disorders, and migraine headaches; (6) major inflammatory disorders, heart failure, and chronic lung disease; or (7) hormone replacement therapy in female participants. The included participants were screened to ensure group status as listed below:

- CTL: Participants had a mean systolic BP ≤ 140 mmHg, a mean diastolic BP ≤ 90 mmHg, no history of antihypertensive medication use, and a fasting glucose level (FGL) ≤ 6.1 mmol/L.
- HT: Participants were using antihypertensive medication under physician prescription for a minimum of two years, with current blood pressure within a normal or HT range and limited to those who were using long-acting antihypertensive medications (e.g., ACEIs, angiotensin II receptor blockers, diuretics) in order to capture the most commonly prescribed medications.
- HT + DM: Participants had a physician diagnosis of type 2 DM for a duration of at least two years, were controlling their DM through diet or hypoglycemic medication alone, and were free of major DM

complications as defined in the exclusion criteria, in addition to the criteria for the HT.

Data on the use and duration of all medications and the disease duration of HT and DM were collected. Participants provided a fasting blood sample for measurement of hematocrit, lipid profile (triacylglycerides (TG), total cholesterol (TC), low-density lipoprotein (LDL), and high-density lipoprotein (HDL)), CRP, glucose, insulin, and HbA1c. Blood pressure, weight, height, and waist circumference were also measured. These measurements were followed by a practice session of the breath hold task in an MRI simulator to ensure that the participant was comfortable with the fMRI scanning protocol. Participants were asked to continue their usual diet, medications, and activity level for the duration of their involvement in the study. Available data from 56 participants (CTL:21, HT: 23, and HT + DM: 12) were preprocessed as described below. Data from seven participants (CTL:3, HT:3, and HT + DM:1) were removed from analysis due to excessive head-motion artifacts larger than 1° rotation and 1 mm translation as detected by FSL motion correction. This study consisted of remaining data from 49 participants (CTL: 18, HT: 20, and HT + DM: 11) with mean ages of 70.2 ± 3.3 , 71.9 ± 4.7 , and 71.7 ± 3.6 years, and male/female ratios of 1.25, 0.43 and 0.57, respectively.

Data acquisition

Each participant followed a set of 6 repetitions of a 30 s resting and 2 s exhale followed by a 15 s BH guided by visual clues (total duration, $T=47$ s) during a dual-echo pCASL fMRI image acquisition session on a Siemens Trio 3T system (T2*-weighted echo-planar imaging, FOV = 220 mm, acquisition matrix = 220×220 , voxel size = $3.4 \times 3.4 \times 6.0$ mm, bandwidth = 2790 Hz/Pixel, TE1/TE2/TR = 9.1/25/4000 ms, flip angle = 90 degrees, slices = 16, averages = 1, concatenations = 1, scan duration = 5:24). The labelling duration was 1500 ms, and the post-labelling delay was 1000 ms. The data associated with the second TE were used to compute the BOLD time series. Respiratory bellows were recorded using the scanner's built-in belt. A T1 anatomical scan (FOV = 256 mm, acquisition matrix = 192×256 , voxel size = 1.0 mm^3 , bandwidth = 200 Hz/Pixel, TI/TE/TR = 1100/2.63/2000 ms, flip angle = 9 degrees, slices = 160) was acquired for anatomical reference and tissue segmentation.

Preprocessing

The dual-echo pCASL time series data were preprocessed using FSL^{35,36} and AFNI^{37,38} tools, and steps

include slice timing correction, motion correction (for the BOLD echo separately and registration into MNI space using *flirt*). The BOLD time series was obtained by surround averaging to produce 78 frames of BOLD data, which were then high-pass filtered to remove low-frequency noise from the data with a 0.01 Hz cut-off frequency, resulting in the “preprocessed BOLD signal”.

Data-driven CVR estimation: amplitude and lag

Previous work demonstrated that the BH CVR response can be successfully approximated as a sinusoidal signal by assuming the BH task is approximately symmetrical (equivalent BH and baseline periods), even if it is not.^{5,27} The sinusoidal regressor outperformed block-design regressors (convolved with the hemodynamic response function), prompting us to visualize the CVR estimation in the Fourier domain. Indeed, identifying the maximum cross-correlation between the BOLD signal and a sinusoidal regressor is mathematically equivalent to extracting the spectral coherence of the BOLD signal and the sinusoid at the nominal task frequency that characterizes the sinusoid. Since the Fourier transform of a sinusoid is a delta function, the coherence function reduces to the Fourier transform of the BOLD signal. In our case, instead of focusing on the nominal task frequency, we extract the peak frequency from the BOLD signal. The phase angle of the Fourier transform at the estimated BH frequency is taken to represent the voxel-wise CVR lag. A biologically meaningful lag, however, needs to be estimated from a reference phase that reflects the time at which the CVR effects first entered the brain. One choice is to get the reference from PETCO₂ or respiratory belt signals, but these signals are not always available. Moreover, a lag referenced to these signals incorporates the transit delay from the lungs to the brain instead of reflecting the brain-tissue specific lags. This hampers the detection of negative CVR, which are in theory at a phase between π and 2π relative to the “earliest arrival time” of the CVR effect in the brain. In response, one can try to isolate the BOLD signal at the internal carotid as an “earliest arrival” signal, but localizing major arteries solely from BOLD data is not always possible due to poor resolution or the lack of coverage of the base of the brain. We propose that the global BOLD signal, which represents an intermediate point of arrival for the CVR effects and has shown considerable similarity between participants in resting state fMRI studies,³⁹ can be leveraged to estimate the “earliest arrival” time.

The CVR estimation pipeline is shown in Figure 1. The BOLD data is first normalized by the mean of the first 8 frames of the series corresponding to the baseline before the first BH period. The time series data was

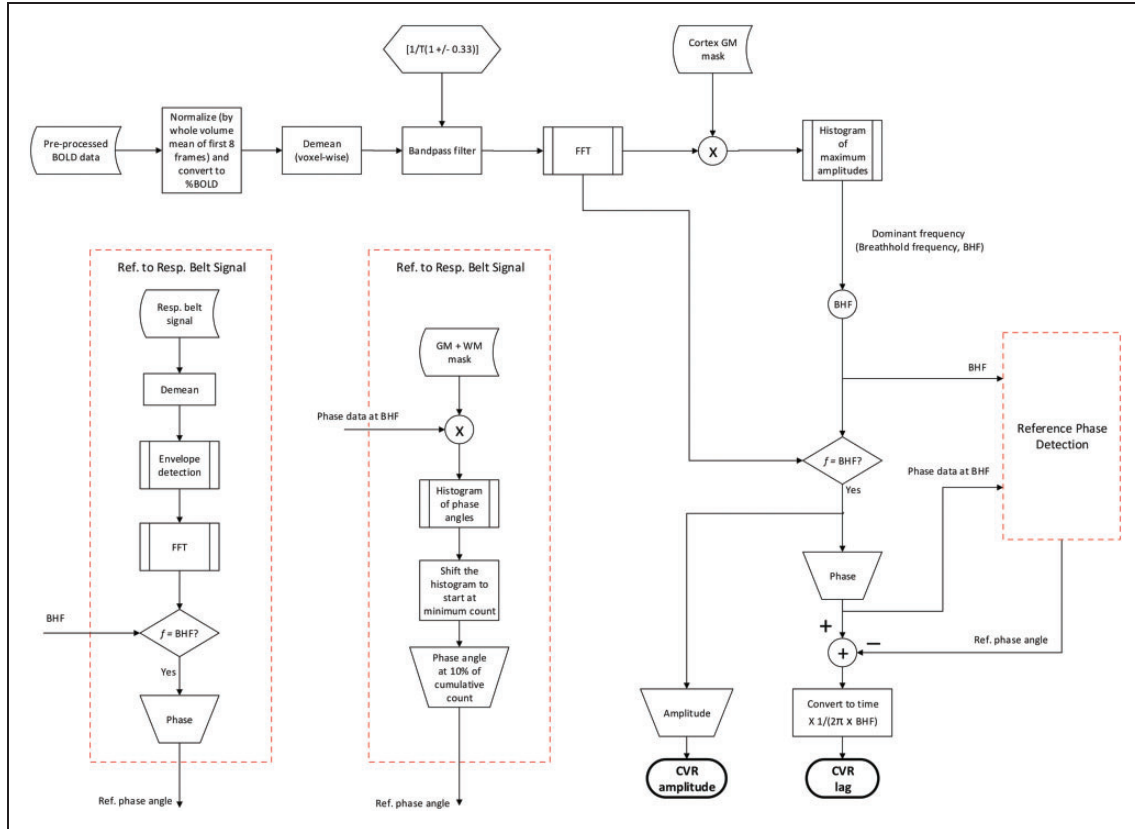


Figure 1. Signal processing pipeline. The normalized and demeaned $\% \Delta \text{BOLD}$ data are bandpass filtered to retain signals around the targeted BH frequency (BHF). The dominant frequency of the filtered signal in the cortex is selected as the BHF. The amplitude of the spectrum of each voxel at the BHF is selected as the CVR amplitude. The CVR lag of each voxel is calculated relative to a reference phase angle. We propose to use the GMS to extract the reference phase angle, the results of which are compared to those of an alternate reference, in this case, the respiratory belt signal at the BHF.

then converted to $\% \Delta \text{BOLD}$ by voxelwise demeaning. As described earlier, the identification of the BH frequency (BHF) can be hampered by variations in task compliance as well as in participant physiology. Thus, the identification of the BHF in our pipeline undergoes a two-step process to ensure flexibility and robustness. First, we identify the BH task paradigm used in the study that can be considered as a repetitive signal of period $T = 47$ s, corresponding to a fundamental BHF of $\frac{1}{T}$ (0.0213 Hz). The voxelwise BOLD signal was passed through a bandpass filter of cut-off frequencies $\left[\frac{1}{(T+0.33T)}, \frac{1}{(T-0.33T)} \right] = [0.0158, 0.0323]$ Hz, corresponding to $T \pm T/3$. The pipeline finds the BHF from the BOLD data spectrum within this frequency range, such that the BHF can deviate slightly from the nominal frequency due to variations in participant compliance with the task design, but is not allowed to deviate too far away from the expected task frequency to ensure robustness against noise. Second, the pipeline finds the BHF corresponding to the maximum amplitude of the Fourier spectrum of the BOLD signal at each cortical voxel. Lastly, for the grey matter (GM) of

each data set, a histogram is constructed using the voxel-wise BHF, and the BHF found at the peak occurrence is chosen as the dominant BHF for that data set. This second step further constrains the BHF to maximize inter-regional comparability, assuming that variations in respiratory physiology contribute to inter-participant but not within-participant inter-regional CVR differences. That is, the dominant BHF can vary between participants but not between brain regions.

The voxelwise phase (ϕ_s) of the CVR at BHF relative to a reference at the same frequency can be used to compute the response lag for the CVR response. For reasons mentioned earlier, a reference that reflects the CO_2 stimulus specific to the brain is desirable. Thus, we propose that it is more feasible to use the BOLD distribution signal phase at BHF of the GMS (based on all GM and white matter (WM) voxels) to estimate the reference phase angle.

- Global-mean signal (GMS) reference: The histogram of the phase angle distribution of the Fourier spectrum of the BOLD signal in the whole brain

(total GM and WM) region is created with a bin size of $\pi/36$ rad. The histogram is then shifted to start at the phase angle bin corresponding to the minimum count. The selected minimum phase angle (ϕ_m) at 10% of the cumulative distribution of shifted phase angles is selected as the reference phase for the CVR lag calculation (see sample phase distribution in Supplementary Figure S1).

$$\text{CVR lag} = \frac{(\phi_s - \phi_m)}{2\pi \times \text{BHF}} \quad (1)$$

CVR amplitude values in voxels with lags longer than 23.5 s (corresponding to a phase lag of π) are considered negative.

In this work, we cross-validate the GMS-based lag values through correlation with lags estimated using a respiratory recording as the reference.

- **Respiratory-belt signal as reference:** the envelope of the respiratory signal is extracted from the recording, which also allowed us to verify each participant's compliance with the BH task. The phase (ϕ_r) of the de-meaned respiratory belt signal envelope Fourier spectrum at the BHF is selected as the reference for CVR lag, calculations as

$$\text{CVR lag} = \frac{(\phi_s - \phi_r)}{2\pi \times \text{BHF}} \quad (2)$$

Statistical analysis

We also computed the Framingham Risk Score (FRS)⁴⁰ and Diabetes Epidemiology: Collaborative Analysis of Diagnostic Criteria in Europe (DECODE) scores.⁴¹ FRS and/or DECODE scores are widely used in cardiovascular disease (CVD) risk estimates to decide on therapeutic strategies for patients at risk of CVD events. Higher values for these scores indicate an elevated risk of such events. Differences in demographics and physiological measurements across groups, including the FRS and DECODE metrics, were detected by ordinary one-way ANOVA corrected for multiple comparisons by controlling the false discovery rate using the Benjamini-Hochberg procedure.

The CVR amplitude and lag were compared voxel-wise and region-wise across the three groups (namely CTL, HT, and HT + DM) using GLM⁴² followed by multiple comparisons correction via threshold-free cluster enhancement.⁴³ Brain parcellations were generated using FreeSurfer (Version 6.0.1, available at surfer.nmr.mgh.harvard.edu) were used to calculate regional-mean CVR amplitudes and mean CVR lags.

The normality of data distributions in all three groups were confirmed using the D'Agostino-Pearson test.⁴⁴ Two-way ANOVA with multiple comparisons was used to separately compare the overall means of region-wise (ROI) CVR amplitude and lag corrected for multiple comparisons by controlling the false discovery rate (Benjamini-Hochberg procedure) between groups. Regional CVR amplitude and lag were compared separately in each cortical region of interest (ROI) using the Kruskal-Wallis test corrected for multiple comparisons by controlling the false discovery rate.

Results

The age of participants was not significantly different across the groups (see Supplementary Figure S2a). HT and HT + DM groups did not exhibit significant differences in systolic BP (SBP) compared to CTL (Supplementary Figure 2b). Participants in HT and HT + DM were using antihypertensive medication under physician prescription for a minimum of two years. Hence their hypertension is mostly controlled showing no statistically significant difference in the SBP to participants in CTL. The HT + DM group showed significantly higher HbA1C and lower LDL cholesterol values compared to the HT and CTL groups (Supplementary Figure 2c, d). The FRS and DECODE scores were both significantly lower in CTL compared to HT and HT + DM, but only the DECODE score showed a significantly lower score for HT compared to HT + DM (Supplementary Figure 2e, f).

Robustness to participant compliance

Shown in Figure 2 are sample signals from the intermediate steps of the signal processing pipeline for a participant compliant (2a) and a participant non-compliant (2b) to the BH task design. Bandpass filtering suppressed spurious signals outside the targeted BHF range, as in Figure 2a(ii) and b(ii). The histograms of maximum amplitudes of the bandpass-filtered BOLD spectra in all cortical voxels are shown in Figure 2a(i) and b(i) for sample participants. The peaks of the histograms correspond to the dominant CVR frequencies. In addition, the BOLD signal at the dominant frequency is well-modelled by the sinusoidal approximation and closely follows the respiratory belt signal as shown in Figure 2a(v) and b(v), even when the participant performance on the BH task deviated from the task design.

Figure 2 also shows the recorded full respiratory-belt signal and the extracted BH pattern from the smoothed envelope details with corresponding frequency spectrums for a participant who followed the BH task paradigm (Figure 2a(iii) and (iv) respectively)

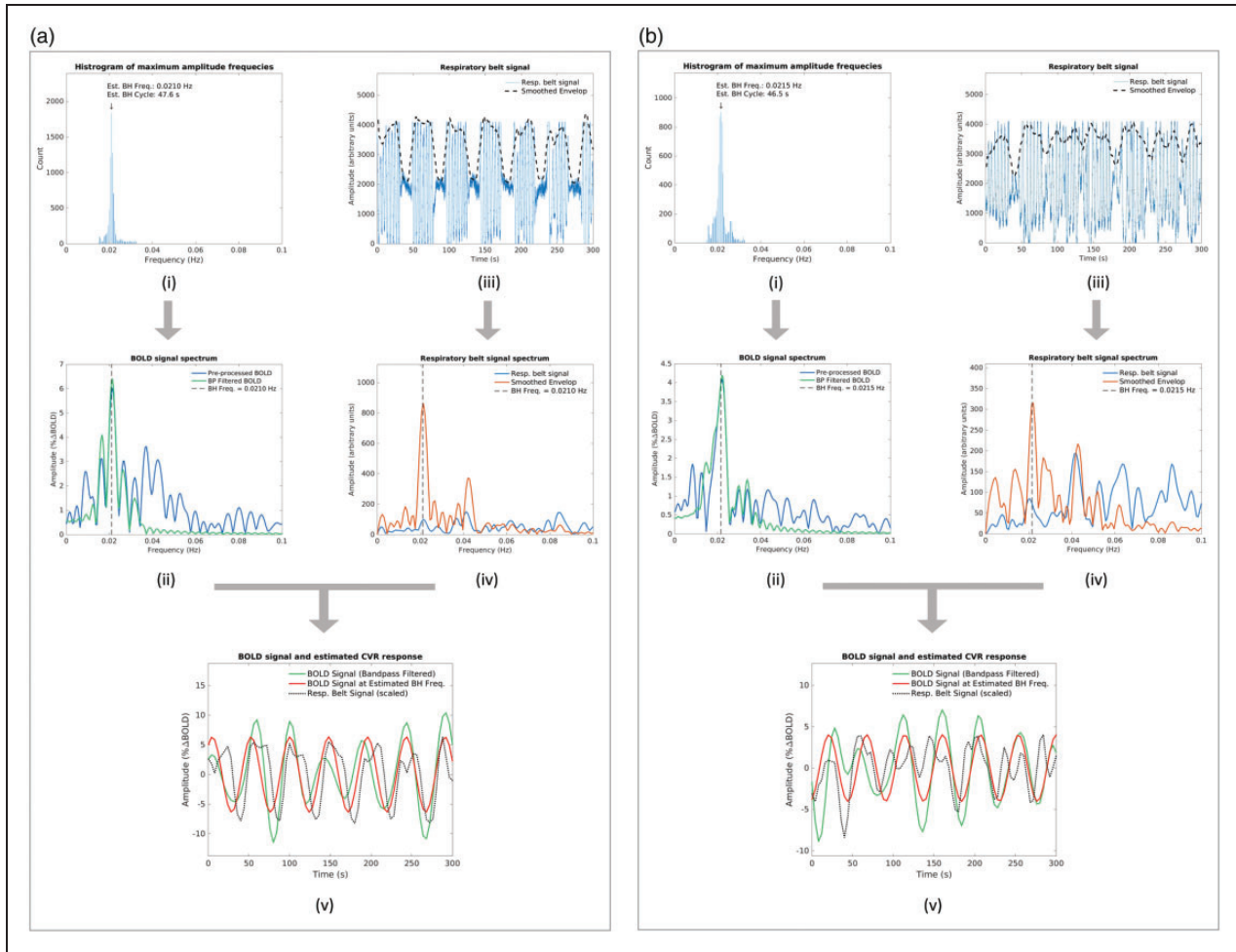


Figure 2. Samples outputs from intermediate signal-processing steps. Samples from the signal processing pipeline for a participant (a) compliant and (b) non-compliant to BH task design. Each includes (i) the histogram of maximum amplitudes at all cortical voxels with corresponding frequencies, (ii) the frequency spectrum of the pre-processed and band-pass filtered BOLD at a sample voxel in the cortex, (iii) the respiratory belt signal with the smoothed envelope, (iv) respective frequency spectrum of the belt signal, and (v) bandpass filtered the BOLD signal, and the estimated CVR response at the BHF at the sample voxel in the cortex.

and for a participant who was not compliant (Figure 2b(iii) and b(iv) respectively). As indicated by dashed lines on respective frequency spectrums, the proposed data-driven approach was able to correctly estimate the BHF in both cases avoiding peaks from unexpected frequencies.

Comparison of GMS- and belt-based lag estimates

Figure 3 shows a high correlation between the CVR lag calculated using the references estimated from the selected minimum phase angle of the GMS phase distribution and from the respiratory belt signal. That is, irrespective of the actual lag values, the relative patterns of GMS-based and belt-based lags agree. This finding establishes the feasibility of voxel-wise CVR lag estimation solely from the BOLD data without a requirement to collect any other external signal and

enables us to map negative CVR values using Fourier data alone. We use the selected minimum phase angle of the GMS phase distribution for all analyses reported in the paper.

Comparison of group-mean maps

Figure 4(a) shows the mean CVR amplitude maps in each group. GM regions in the cortex generally have a higher CVR amplitude compared to other areas of the brain. The mean CVR amplitude in CTL was significantly higher than both HT and HT + DM across cortical GM and higher in HT compared to HT + DM (see supplementary Figure S3a). Note that CVR amplitudes in voxels with lags longer than 23.5 s (corresponding to a phase lag of π) are considered negative (shown in blue). We illustrate the occurrence of negative CVRs in the medial prefrontal region. Lags are shortest in the

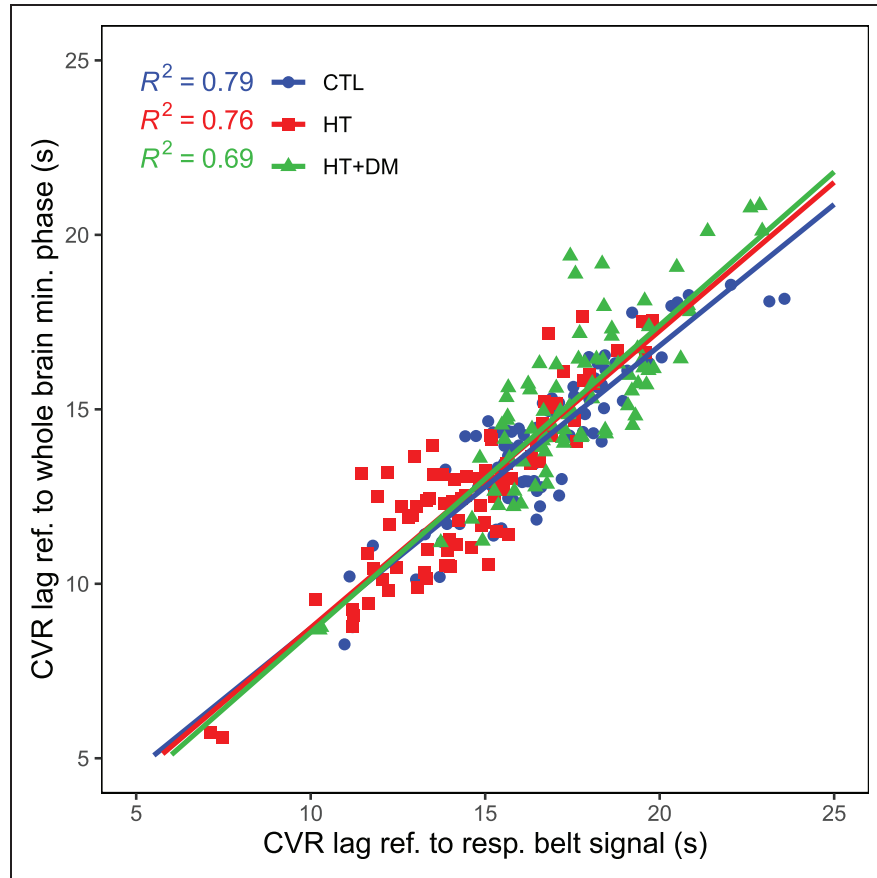


Figure 3. The relationship between CVR lag calculated using the references estimated from the selected minimum phase angle of the GMS phase distribution and the respiratory belt signal shows a high correlation. Each symbol represents the group average for each ROI.

occipital lobe and longest in the ventricles and WM. In the remainder of the results, we only compare the magnitudes of CVR values across groups, which means we do not restrict lags to a phase of π . We believe this approach is more generalizable than comparing positive CVRs against negative CVRs. Nonetheless, regions associated with negative CVR are represented by phases of $>\pi$ (i.e. $>$ lags of 23.5 s).

Figure 4(b) shows the mean CVR lag maps in each group. GM regions in the cortex generally have a shorter delay than in other areas of the brain. The mean CVR lag in HT + DM was significantly longer than both CTL and HT across cortical GM and longer in CTL compared to HT (see supplementary Figure S3b).

Voxel-wise associations with disease variables

Figure 5 shows voxels that demonstrate statistically significant differences ($p < 0.05$) where CVR magnitudes in CTL $>$ HT and CTL $>$ HT + DM. Most CVR amplitude differences are either reduced or eliminated when controlling for sex, duration of previously detected hypercholesterolemia, or systolic blood

pressure. No statistical significance voxels were detected when controlling for LDL or HbA1c. No significant voxelwise differences in CVR magnitude were detected between HT and HT + DM.

Figure 6 shows voxels that demonstrate statistically significant differences ($p < 0.05$) where CVR lags in CTL $>$ HT and HT $<$ HT + DM. More significant differences were detected for HT $<$ HT + DM than CTL $>$ HT and those differences were reduced when controlling for the duration of previously detected hypercholesterolemia and disappeared when controlling for LDL and HbA1c. Significant differences in CVR lag were not detected between CTL and HT + DM.

There is no statistically significant association of CVR amplitude or lag with FRS or DECODE scores detected between groups.

ROI-based differences between groups

Figure 7(a) shows the regional means of CVR magnitude and lag of each cortical ROI for CTL, the regional means of CVR magnitude (b) and lag (c) of each

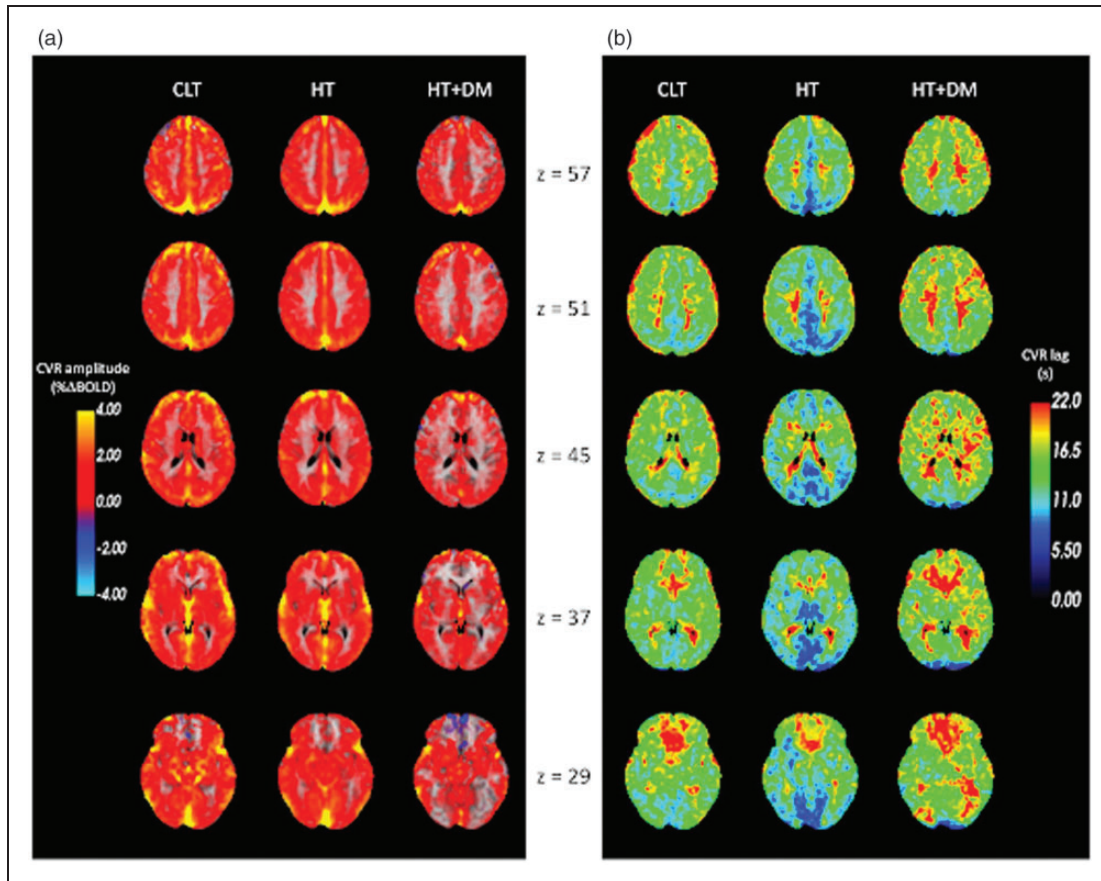


Figure 4. Group-mean CVR estimation results sampled to MNI space. (a) Mean CVR amplitudes (% Δ BOLD) for all participants in each group. CVR amplitude values in voxels with lags longer than 23.5 s (corresponding to a phase lag of π) are considered negative. The grey matter (GM) regions in the cortex have a higher CVR amplitude than the white matter (WM) and other areas of the brain. The HT + DM participants showed the lowest CVR amplitudes consistently throughout all brain regions and (b) Mean CVR lag (s) relative to the GMS min phase in each group. The GM regions in the cortex have a shorter CVR lag than the WM and other areas of the brain. The HT group showed the lowest CVR lag while the HT + DM group showed the longest lag. Parts of the ventricles are masked out indicated as zero for both CVR amplitude and lag to aid the visualization, but CVR was estimated in all voxels. The z value indicates slice coordinates in MNI152 space.

cortical ROI for HT and HT + DM. CVR magnitude in HT + DM is significantly lower than both CTL and HT in the cuneus, the pericalcarine, the lingual, the lateral occipital, and significantly lower than CTL in the posterior cingulate, the fusiform, the pallidum, and the hippocampus. CVR amplitude in HT is significantly lower than both CTL in the pallidum. HT exhibited significantly shorter lags than CTL in the cerebellum cortex, the cuneus, the pericalcarine, the lingual, the superior temporal, and the rostral anterior cingulate. The CVR lag was significantly longer in HT + DM than HT in the precuneus, the cuneus, the pericalcarine, the caudal anterior-cingulate, the lingual, the posterior cingulate, the banks of the superior temporal sulcus, the fusiform, the superior temporal, the rostral anterior cingulate.

Discussion

In this work, we present a simple, frequency-domain-based, data-driven approach for estimating CVR amplitude and lag from BH fMRI data, helping to reduce errors due to participant non-compliance and regional CVR lag variability. It thus can have a wide range of applications in studying patient populations. Moreover, our Fourier-spectrum approach provides an elegant means to estimate voxelwise CVR lag estimations using phase differences relative to any non-neural biological signal that depends on the BH task.^{7,45} We demonstrate our method in the study of diabetes and hypertension. We found that:

1. It is feasible to use the phase distribution of the BOLD signal relative to a GMS reference to

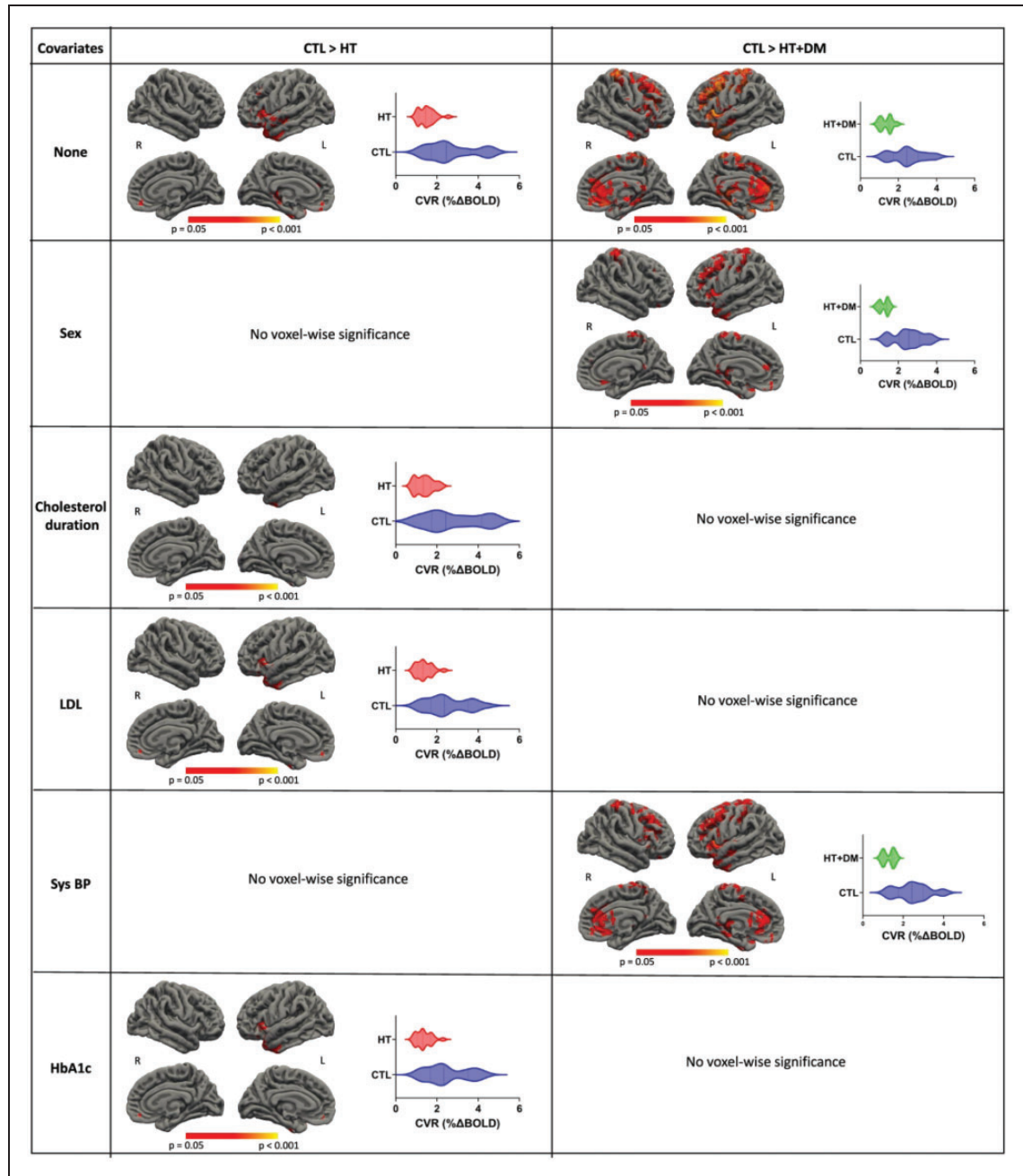


Figure 5. Voxelwise comparisons of CVR magnitudes. The statistical testing on CVR magnitudes of CTL > HT and CTL > HT + DM shows significant voxels ($p < 0.05$) for permutation inference for the general linear model after threshold-free cluster enhancement. The values in the significant ROIs are shown in the corresponding violin plots. The significance of differences in most voxels is either reduced or eliminated when controlled for other variables. Significant differences in CVR amplitude were not detected between HT and HT + DM.

- estimate brain-specific CVR lags, and to use these lags to detect the presence of negative CVR;
- CVR lag is a more sensitive marker of differences between CTL and patient groups than CVR magnitude;
- HT is associated with comparable regional CVR magnitudes as CTL, but shorter CVR lags;
- HT + DM is associated with lower regional CVR magnitudes than both HT and CTL as well as longer CVR lags relative to HT but not CTL;

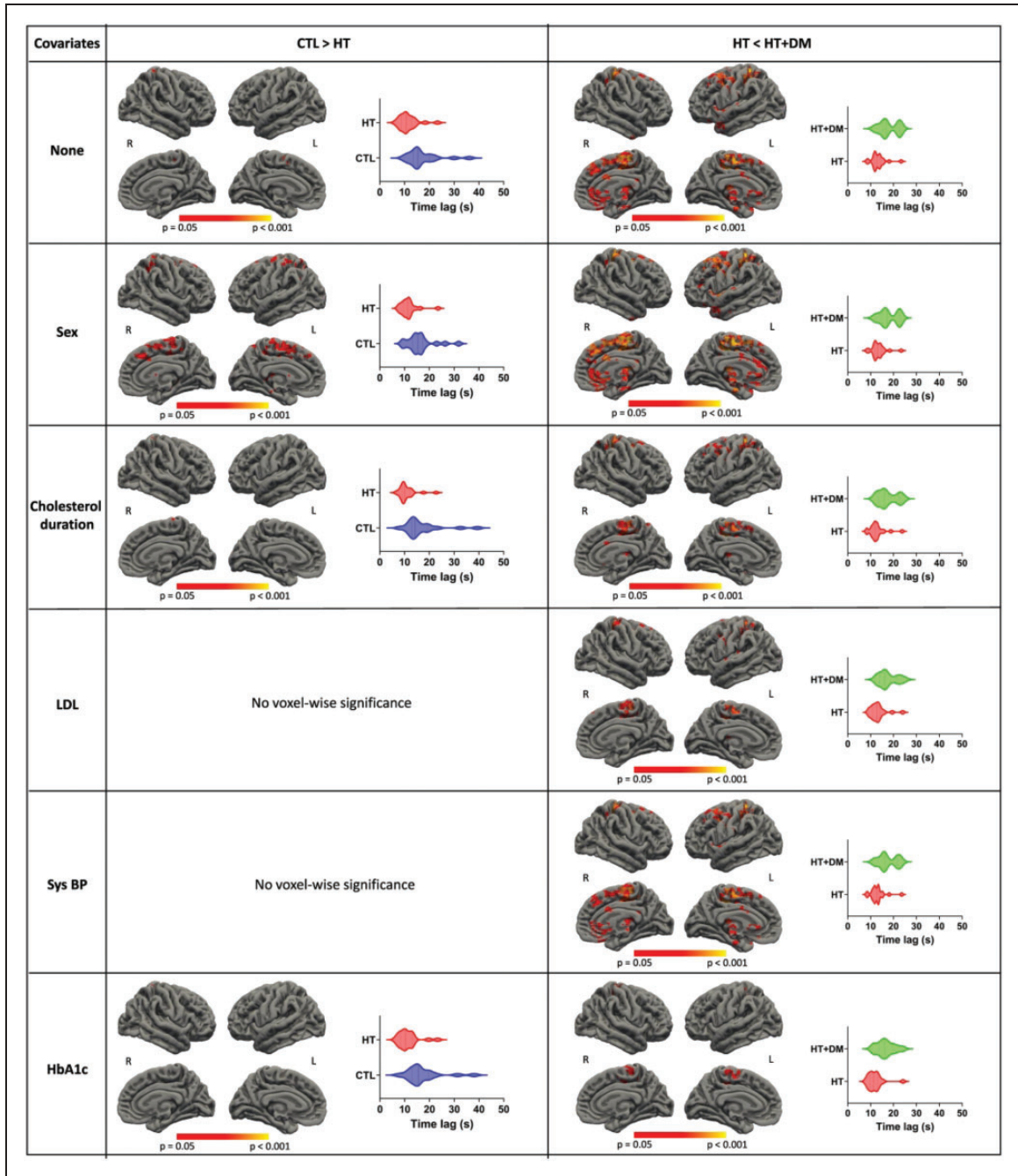


Figure 6. Voxelwise comparisons of CVR lag. The statistical testing on the CVR lag of CTL > HT and HT < HT + DM showed significant voxels ($p < 0.05$) for permutation inference for the general linear model after threshold-free cluster enhancement. More significant differences were detected for HT < HT + DM than for CTL > HT; these were reduced when controlling for the duration of previously detected hypercholesterolemia and disappeared when controlling for LDL and HbA1c. Significant differences in CVR lag were not detected between CTL and HT + DM.

5. CVR lag differed between groups in more brain regions than CVR magnitude.

These are the first MRI-based observations of CVR lag differences between HT-DM patients and healthy controls.

Estimation and interpretation of CVR amplitude using BH

A BH task is a simple method to induce cerebrovascular response due to an increase of arterial CO_2 levels by ceasing ventilation. It provides a reproducible

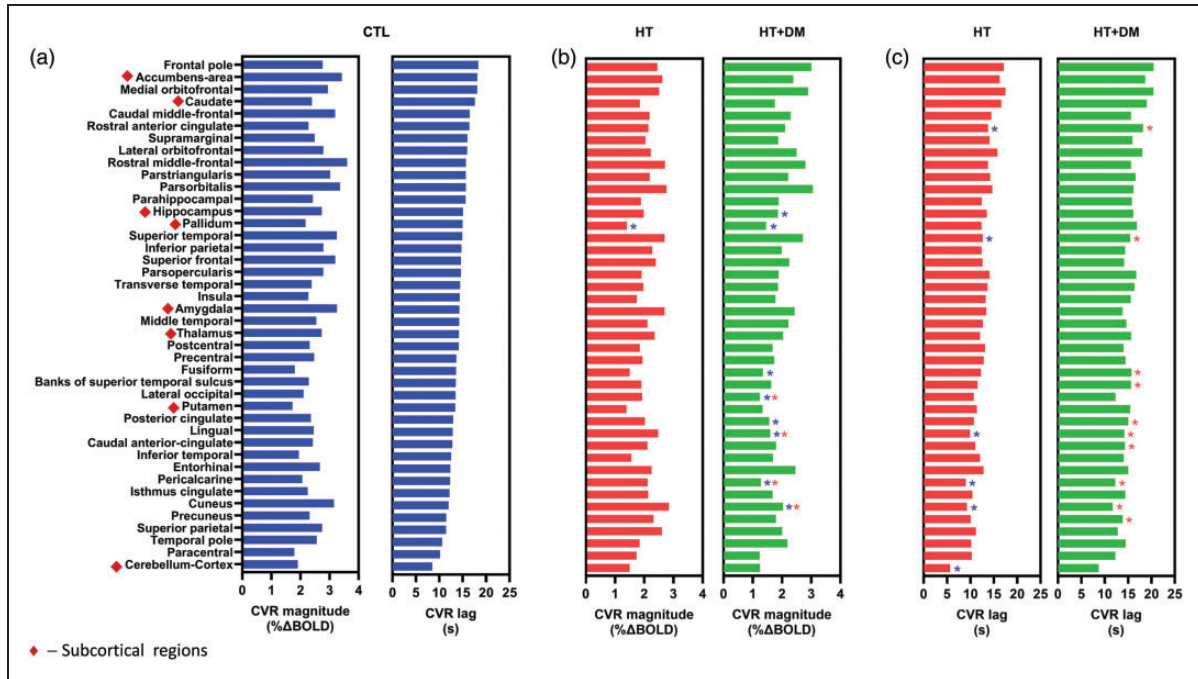


Figure 7. (a) Mean regional CVR amplitude and lag for CTL arranged in the ascending order of CTL in subregions of the cortex. The order of CVR magnitudes does not show any link to CVR lag in different subregions. Mean regional CVR (b) magnitude and (c) lag for HT and HT + DM groups arranged in the same ascending order of CTL CVR magnitude. HT + DM shows statistically significant lower CVR magnitudes ($p < 0.05$) in multiple cortical regions than both CTL and HT, marked by blue (*) and red (*) asterisks, respectively. The Kruskal-Wallis test corrected for multiple comparisons by controlling the false discovery rate. The CVR lag shows statistically significant differences in more regions than those for magnitude. Statistically significant shorter CVR lag compared to CTL is marked with blue asterisks (*), and longer CVR lags compared HT are marked by red (*) asterisks. Subcortical regions are marked by diamonds (◆).

technique estimation of CVR even in less cooperative populations.^{5,13,46} The BH-induced CVR has been shown to be comparable to CVR estimated with inhaled CO₂ challenges.^{9,47–49} In the conventional, GLM-based method, the block BH design is convolved with the hemodynamic response function.^{25,26} The GLM models perform well when PETCO₂ recordings are available for modelling BOLD response to accommodate for inter- and intra-participant variations,^{4,14} but may be sensitive to non-compliant participants.²⁸ BOLD fMRI signal changes due to head motion, confounding physiological fluctuations, and other sources of noise can all affect the CVR estimation from BH BOLD data.^{32,50,51}

Alternatively, Fourier basis modelling has been used effectively, assuming sinusoidal signal variations at the paradigm design frequency.^{4,14,27} Fourier-based approaches have been reported as being robust and versatile, but are seemingly more ideal for BH designs that are symmetrical. In practice, the BOLD response to BH tasks can easily deviate from the sinusoidal frequency, and it is unclear what the implications are for CVR estimation.

In our data-driven approach, we addressed this issue by estimating fundamental frequency from the BOLD signal spectrum for accurate sinusoidal approximation of CVR. GM regions in the cortex generally have a higher CVR amplitude (Figure 3) than the WM and other areas of the brain. Regional variations within the GM are also visible. Frontal regions generally have a higher CVR amplitude compared to temporal regions, the cerebellum cortex, the fusiform, and the putamen. These overall and regional differences are consistent with previous similar studies,^{32,52,53} and attest to the robustness of our simple approach.

CVR amplitude in diabetes and hypertension

CVR changes have been reported in various chronic conditions.^{10,20,54–57} Chronic hypertension⁵⁸ has been associated with CVR impairments.^{54,56,57,59,60} Specifically, in HT, CVR is extensively reduced in hypertensive rats compared to controls.⁵⁷ In older adults, HT is well known to be associated with arterial stiffness and blood-flow reduction⁶¹ in addition to reductions in whole-brain CVR.⁶² This CVR reduction is also

reflected in reduced resting-state fMRI signal fluctuations across the brain in the presence of arterial stiffness.⁶³ The reduced CVR is in turn associated with impaired executive function,⁶⁴ and can be attributed to shear stress on the endothelial membrane that contributes to atherosclerosis.⁶⁵ In the current study, however, CVR amplitude was not significantly altered in the HT group – we observed lower CVR magnitude in HT in the pallidum alone. This leads us to think that the incorporation of voxel-wise CVR lags, which had not been done in previous studies, may have led to the underestimation of CVR in HT previously. Our results suggest that HT is rather associated with CVR lag. This is consistent with the higher pulse-wave velocity and less dampened HRF that we expected from stiff vessels. There was minimal evidence of sex differences in the CVR impairment, perhaps due to the limited sample size.

Diabetes mellitus (DM) and HT are commonly comorbid, and vascular dysfunction has long been known as a part of DM pathology. Thickening of the vascular membrane has been identified as one of the hallmarks of DM, associated with reduced vascular elasticity.^{66,67} Using transcranial Doppler ultrasound (TCD), CO₂-based CVR in the middle-cerebral artery was found to be impaired in DM.⁶⁰ However, studies of the effect of DM on CVR in human populations are still scarce. Ivankovic reported TCD-based vascular reactivity reductions,⁵⁴ echoing findings in the rat model. Our previous study was one of the few human MRI studies of DM + HT used the BH challenge, and localized the CVR deficit to the occipital lobe.¹¹ Like HT, DM is also associated with blood-flow impairment^{68,69} as well as psychological symptoms, such as depression.⁶⁸ Damage of the proximal tubule, involved in the uptake of vascular endothelial growth factor (VEGF),⁷⁰ as well as a reduction in the brain-derived neurotrophic factor (BDNF),⁷¹ have been implicated in vascular and cognitive pathologies in DM, respectively. In the current study, CVR amplitude was found to be significantly reduced in the frontal, precuneus, posteriorcingulate and pericalcarine regions (Figure 5). The implicated regions are known to exhibit high rates of metabolism⁷² and consequently, high blood flow,⁷³ rendering them more susceptible to vascular damage. Abnormalities in regions is also consistent with functional impairments reported in previous studies.¹² Like in the case of HT, there is minimal evidence of sex differences in the CVR impairment.

Estimation and interpretation of CVR lag

In addition to CVR amplitude, CVR lag is increasingly quantified.^{52,74–78} Specifically, Holmes et al. demonstrated extended CVR lag as a marker with superior sensitivity to the effects of age and Alzheimer's disease,

even when compared to the long-established CVR amplitude measures.⁷⁹

The BOLD temporal-lag structure has also been estimated in the resting-state BOLD signal by regressing the low-frequency (~0.1 Hz) arterial BOLD signal,⁸⁰ venous BOLD signal^{81,82} or GMS.^{83,84} It is understood that the BOLD signal is an indirect measure of blood traversal, as it reflects variations in both blood volume and blood oxygenation, which may change due to neuronal activity as well. An alternative is to track the BOLD signal change during a hyperoxic or hypercapnic hyperoxic (i.e. carbogen) gas challenge.⁸⁵ This latter alternative is easier to administer clinically than blood tagging while eliciting a generally robust BOLD response.⁷⁴ Indeed, CVR-lag estimation is more robust when performed for a respiratory challenge than using resting-state data.^{77,86,87}

The BH task has previously been used for CVR-lag mapping.^{20,32,88} Moreover, the use of Fourier analysis to elegantly estimate the BOLD-CO₂ response lag was previously proposed with the use of a sinusoidal CO₂ stimulus.⁴⁵ It was noted that head motion could negatively affect the accuracy of CVR lag estimation when using BH BOLD fMRI.³² The delay times are most commonly estimated as the time shift corresponding to the maximum cross-correlation or most significant linear regression in a GLM between the reference and the BOLD signals, with the reference signal being: (1) the PETCO₂ recording, (2) the whole-grey-matter (GM) BOLD signal,^{31,80} and (3) the respiratory variability signal (RVT).⁸⁶

In our work, we propose a GMS-based CVR lag estimation method, which is successfully cross-validated with the respiratory-belt reference. However, unlike GLM-based approaches, no assumptions about the HRF are required in our approach. Moreover, consistent with previous work demonstrating the advantages of voxel-wise sinusoidal BOLD response frequency and phase adjustments,³¹ our method was able to achieve robust CVR lag estimates. Pinto et al. added higher-frequency harmonics to the original single-frequency sinusoidal regressor and demonstrated improvements in CVR model fits.¹⁴ Equivalently, if needed, our method could easily incorporate the phases of higher-frequency spectral peaks in the lag calculation. Our chosen GMS reference foregoes any need for external recordings, and bypasses challenges posed in poor recording quality.⁸⁶ The CVR lag thus calculated conveniently allows us to detect negative CVR based on a phase value being between π and 2π , but it is not equivalent to the RVT reference, which embodies the transit time for the CO₂ bolus to reach the brain, in addition to any regional specific CVR delays. The former reflects both systemic blood-flow velocity and transit through

the main cerebrovascular arteries, while the latter reflects localized vascular elasticity.

In our work, CVR lag in healthy adults spans the range of 10–15 s in the GM. Frontal cortical regions and deep-grey regions exhibit the longest CVR lags, while the temporal and parietal regions tend to exhibit shorter lags. These observations are consistent with the work of Trippleton et al.⁵² The long lags observed in ventricular regions are consistent with negative lag-free CVR observed in these regions in other studies.⁸⁹ However, while many publications show maps of CVR lag, few quantify regional differences, limiting our ability for cross-validation. The observed spatial diversity in CVR lag may in part be driven by differences in flow patterns in various cerebrovascular territories, including flow transit time and dispersion among others. The temporal and frontal regions, for instance, are supplied by different arterial offshoots, and borrowing from the arterial-spin labelling literature, arterial transit time from the base of the brain is thought to be longest in the occipital region and shortest in deep GM, with flow dispersion following a similar pattern.⁹⁰ Thus, we are led to think that vascular anatomy is not the main driver of these regional lag differences, but rather, CVR lag is driven by regional vascular elasticity. This supports the utility of CVR lags as potential early indicators of regional physiological integrity.

CVR lag in diabetes and hypertension

DM is well associated with reduced systemic⁹¹ and cerebral blood flow velocity.^{68,92} Reports of CVR amplitude deficits have implicated the bilateral occipito-parietal regions.¹¹ In this work, the main DM-related finding is that CVR lag is a more sensitive marker of diabetes than CVR amplitude, as DM + HT participants exhibited longer CVR lags than HTs in more GM regions than did CVR magnitude (Figure 7), and CVR lag was associated with more disease-related variables than amplitude (Figure 6). The lengthened CVR lag can in part be attributed to the reduced systemic blood-flow velocity,⁶² but more likely slowed local HRF due to cerebrovascular damage stemming such factors as hyperglycemia⁶⁷ and the reduction of the blood-derived neurotropic factor.⁷¹ These in turn impair endothelial repair and survival⁹³ in what is potentially a vicious cycle akin to those of other processes such as Alzheimer's disease and aging.⁹⁴

One striking finding in this work is that the CVR lag is generally shorter in the HT group than in either the CTL or HT + DM group. In contrast, there was negligible significant difference in CVR amplitude between the HT and CTL groups (Figure 7), suggesting that a healthy CVR amplitude may belie early endothelial

pathology⁶⁵ and that using CVR amplitude alone may lead to missed opportunities for understanding the cerebrovascular mechanisms of HT. While counter-intuitive, the finding of reduced CVR delay in HT is consistent with prior ultrasound-based reports of increased blood-flow velocity in the presence of elevated blood pressure.⁹⁵ Hypertension is often comorbid with diabetes mellitus.⁵⁴ However, it is common for diabetes patients to receive hypertension treatment, and as demonstrated in this work, the effect of DM on CVR lag in the DM + HT group surpasses that of HT alone.

Given that our HT patients are medicated for at least 2 years, the effects of common anti-hypertensive medications should also be discussed. ACEIs (ACE inhibitors) and angiotensin II blockers both lead to vasodilation, which can increase blood flow leading to reduced vascular lag. While we cannot rule out this effect in our HT findings, especially given that the SBP between the HT and CTL groups was not significantly different, we noted that the HT + DM patients, who also have medicated HT, do not display reduced CVR lag. Thus, the effect of HT without DM is likely distinct from that of the HT medication alone.

Interestingly, HT was associated with significantly reduced CVR lag relative to CTL in numerous regions, despite minimal CVR magnitude differences. Taking the findings from CVR magnitude and phase suggests that HT differs from CTL mainly through CVR lag, while HT + DM differs from CTL mainly through CVR magnitude. This is an interesting distinction between the two conditions that could be clinically meaningful.

Limitations

Our data-driven algorithm successfully estimated the fundamental BHF from the BH BOLD data for sinusoidal modelling of CVR for BH paradigms with reasonably similar 'BH' and 'baseline' periods. However, we recognize that many studies may use highly asymmetrical BH timing paradigms that may not be accurately modelled by a sine-cosine function at the fundamental frequency. This can be easily addressed by adding harmonics into the signal as reported previously for sinusoidal modelling.¹⁴

Likewise, while we use a single most common frequency to characterize the CVR for each participant in this demonstrative study, secondary frequencies can be added to the CVR calculation. Nonetheless, in our own secondary analyses including 3 instead of 1 frequency peak for CVR estimation, the CVR amplitude and lag differences between the groups remained unchanged, demonstrating the robustness of choosing a single "representative" BH CVR frequency.

Third, we cross-validated our results against those obtained using a respiratory-belt recording, but could not cross-validate against results based on PETCO₂, as it was not available in this data set. As such, we are also unable to assess the effect of baseline differences in PETCO₂ across participants. However, we think the novelty of using the GMS as a reference merits consideration in light of the cross validation we provided, and plan to include PETCO₂ validation in our future work.

Finally, our sample included a modest number of participants, including a comparatively small DM + HT sample. In practice, it was challenging to meet our recruitment criteria particularly for the HT and DM + HT groups, resulting in a modest sample size. We hope to replicate and expand on our findings in future studies.

Conclusions

Our algorithm successfully estimated voxel-wise CVR amplitude, magnitude and lag from BH data, supporting a special role for the GMS. The CVR amplitude is estimated in units of %ΔBOLD directly from the data-driven BHF. Serious deviations from the designed task paradigm were suppressed and thus did not bias the estimated CVR values. Our method foregoes the need for externally acquired recordings and can have a wide range of applications in studying patient populations. We demonstrated our method in the study of diabetes and hypertension. The CVR magnitude was lowest in HT + DM, and while CVR lag was lowest in HT. Interestingly, the CVR lag was far more sensitive than the CVR magnitude to differences between HT and HT + DM. These results demonstrate the feasibility of extracting CVR lag using BH challenges and the unique clinical value of CVR lag information.

Data and code availability

The data that support the findings of this study may be made available only according to terms in the research-ethics approval upon request to the corresponding author. The data are not publicly available due to privacy or ethical restrictions. Code will be made available upon request to the corresponding author.

Funding

The author(s) disclosed receipt of the following financial support for the research, authorship, and/or publication of this article: We are grateful to the Canadian Institutes of Health Research (CIHR, FDN 148398) for funding support.

Declaration of conflicting interests

The author(s) declared no potential conflicts of interest with respect to the research, authorship, and/or publication of this article.

Authors' contributions

Nuwan D. Nanayakkara: Conceptualisation, data curation, formal analysis, investigation, methodology, software, validation, visualisation, writing – original draft.

Liesel-Ann Meusel: Data curation, Writing – Review & Editing.


Nicole D. Anderson: Data curation, Writing – Review & Editing.

J. Jean Chen: Conceptualisation, resources, Funding acquisition, data curation, methodology, supervision, Writing – original draft, Writing – Review & Editing.

Supplementary material

Supplemental material for this article is available online.

ORCID iD

Nuwan D Nanayakkara  <https://orcid.org/0000-0001-7125-4479>

References

1. Wise RG, Pattinson KTS, Bulte DP, et al. Dynamic forcing of end-tidal carbon dioxide and oxygen applied to functional magnetic resonance imaging. *J Cereb Blood Flow Metab* 2007; 27: 1521–1532.
2. Mark CI, Slessarev M, Ito S, et al. Precise control of end-tidal carbon dioxide and oxygen improves BOLD and ASL cerebrovascular reactivity measures. *Magn Reson Med* 2010; 64: 749–756.
3. Liu P, Welch BG, Li Y, et al. Multiparametric imaging of brain hemodynamics and function using gas-inhalation MRI. *Neuroimage* 2017; 146: 715–723.
4. Bright MG and Murphy K. Reliable quantification of BOLD fMRI cerebrovascular reactivity despite poor breath-hold performance. *Neuroimage* 2013; 83: 559–568.
5. Lipp I, Murphy K, Caseras X, et al. Agreement and repeatability of vascular reactivity estimates based on a breath-hold task and a resting state scan. *Neuroimage* 2015; 113: 387–396.
6. Urback AL, MacIntosh BJ and Goldstein BI. Cerebrovascular reactivity measured by functional magnetic resonance imaging during breath-hold challenge: a systematic review. *Neurosci Biobehav Rev* 2017; 79: 27–47.
7. Pinto J, Bright MG, Bulte DP, et al. Cerebrovascular reactivity mapping without gas challenges: a methodological guide. *Front Physiol* 2020; 11: 608475.
8. Dlamini N, Shah-Basak P, Leung J, et al. Breath-hold blood oxygen level-dependent MRI: a tool for the assessment of cerebrovascular reserve in children with moyamoya disease. *AJNR Am J Neuroradiol* 2018; 39: 1717–1723.
9. Raut RV, Nair VA, Sattin JA, et al. Hypercapnic evaluation of vascular reactivity in healthy aging and acute stroke via functional MRI. *Neuroimage Clin* 2016; 12: 173–179.
10. Iranmahboob A, Peck KK, Brennan NP, et al. Vascular reactivity maps in patients with gliomas using breath-holding BOLD fMRI. *J Neuroimaging* 2016; 26: 232–239.

11. Tchistiakova E, Anderson ND, Greenwood CE, et al. Combined effects of type 2 diabetes and hypertension associated with cortical thinning and impaired cerebrovascular reactivity relative to hypertension alone in older adults. *Neuroimage Clin* 2014; 5: 36–41.
12. Haight TJ, Bryan RN, Erus G, et al. Vascular risk factors, cerebrovascular reactivity, and the default-mode brain network. *Neuroimage* 2015; 115: 7–16.
13. Peng S-L, Yang H-C, Chen C-M, et al. Short- and long-term reproducibility of BOLD signal change induced by breath-holding at 1.5 and 3T. *NMR Biomed* 2020; 33: e4195.
14. Pinto J, Jorge J, Sousa I, et al. Fourier modeling of the BOLD response to a breath-hold task: optimization and reproducibility. *Neuroimage* 2016; 135: 223–231.
15. Wu P, Bandettini PA, Harper RM, et al. Effects of thoracic pressure changes on MRI signals in the brain. *J Cereb Blood Flow Metab* 2015; 35: 1024–1032.
16. Sousa I, Vilela P and Figueiredo P. Reproducibility of hypocapnic cerebrovascular reactivity measurements using BOLD fMRI in combination with a paced deep breathing task. *Neuroimage* 2014; 98: 31–41.
17. Abbott DF, Opdam HI, Briellmann RS, et al. Brief breath holding may confound functional magnetic resonance imaging studies. *Hum Brain Mapp* 2005; 24: 284–290.
18. Liu H-L, Huang JU-C, Wu C-T, et al. Detectability of blood oxygenation level-dependent signal changes during short breath hold duration. *Magn Reson Imaging* 2002; 20: 643–648.
19. Urbach AL, Metcalfe AWS, Korczak DJ, et al. Magnetic resonance imaging of cerebrovascular reactivity in healthy adolescents. *J Neurosci Methods* 2018; 306: 1–9.
20. Geranmayeh F, Wise RJS, Leech R, et al. Measuring vascular reactivity with breath-holds after stroke: a method to aid interpretation of group-level BOLD signal changes in longitudinal fMRI studies. *Hum Brain Mapp* 2015; 36: 1755–1771.
21. Chang C, Thomason ME and Glover GH. Mapping and correction of vascular hemodynamic latency in the BOLD signal. *Neuroimage* 2008; 43: 90–102.
22. Liu P, Li Y, Pinho M, et al. Cerebrovascular reactivity mapping without gas challenges. *Neuroimage* 2017; 146: 320–326.
23. Tancredi FB and Hoge RD. Comparison of cerebral vascular reactivity measures obtained using breath-holding and CO₂ inhalation. *J Cereb Blood Flow Metab* 2013; 33: 1066–1074.
24. Kannurpatti SS and Biswal BB. Detection and scaling of task-induced fMRI-BOLD response using resting state fluctuations. *Neuroimage* 2008; 40: 1567–1574.
25. Kastrup A, Li TQ, Glover GH, et al. Cerebral blood flow-related signal changes during breath-holding. *AJNR Am J Neuroradiol* 1999; 20: 1233–1238.
26. Biswal BB, Kannurpatti SS and Rypma B. Hemodynamic scaling of fMRI-BOLD signal: validation of low-frequency spectral amplitude as a scalability factor. *Magn Reson Imaging* 2007; 25: 1358–1369.
27. Murphy K, Harris AD and Wise RG. Robustly measuring vascular reactivity differences with breath-hold: normalising stimulus-evoked and resting state BOLD fMRI data. *Neuroimage* 2011; 54: 369–379.
28. Jahanian H, Christen T, Moseley ME, et al. Measuring vascular reactivity with resting-state blood oxygenation level-dependent (BOLD) signal fluctuations: a potential alternative to the breath-holding challenge? *J Cereb Blood Flow Metab* 2017; 37: 2526–2538.
29. Magon S, Basso G, Farace P, et al. Reproducibility of BOLD signal change induced by breath holding. *Neuroimage* 2009; 45: 702–712.
30. Stringer MS, Blair GW, Shi Y, et al. A comparison of CVR magnitude and delay assessed at 1.5 and 3T in patients with cerebral small vessel disease. *Front Physiol* 2021; 12: 644837.
31. van Niftrik CHB, Piccirelli M, Bozinov O, et al. Fine tuning breath-hold-based cerebrovascular reactivity analysis models. *Brain Behav* 2016; 6: e00426.
32. Moia S, Termenon M, Uruñuela E, et al. Ica-based denoising strategies in breath-hold induced cerebrovascular reactivity mapping with multi echo BOLD fMRI. *Neuroimage* 2021; 233: 117914.
33. Birn RM, Smith MA, Jones TB, et al. The respiration response function: the temporal dynamics of fMRI signal fluctuations related to changes in respiration. *Neuroimage* 2008; 40: 644–654.
34. Welsh KA, Breitner JC and Magruder-Habib KM. Detection of dementia in the elderly using telephone screening of cognitive status. *Cogn Behav Neurol* 1993; 6: 103.
35. Jenkinson M, Beckmann CF, Behrens TEJ, et al. FSL. *Neuroimage* 2012; 62: 782–790.
36. Smith SM, Jenkinson M, Woolrich MW, et al. Advances in functional and structural MR image analysis and implementation as FSL. *Neuroimage* 2004; 23 Suppl 1: S208–19.
37. Cox RW. AFNI: software for analysis and visualization of functional magnetic resonance neuroimages. *Comput Biomed Res* 1996; 29: 162–173.
38. Cox RW and Hyde JS. Software tools for analysis and visualization of fMRI data. *NMR Biomed* 1997; 10: 171–178.
39. Erdoğan SB, Tong Y, Hocke LM, et al. Correcting for blood arrival time in global mean regression enhances functional connectivity analysis of resting state fMRI-BOLD signals. *Front Hum Neurosci* 2016; 10: 311.
40. Wilson PW, D'Agostino RB, Levy D, et al. Prediction of coronary heart disease using risk factor categories. *Circulation* 1998; 97: 1837–1847.
41. Balkau B, Hu G, Qiao Q, et al. Prediction of the risk of cardiovascular mortality using a score that includes glucose as a risk factor. The DECODE study. *Diabetologia* 2004; 47: 2118–2128.
42. Winkler AM, Ridgway GR, Webster MA, et al. Permutation inference for the general linear model. *Neuroimage* 2014; 92: 381–397.
43. Smith SM and Nichols TE. Threshold-free cluster enhancement: addressing problems of smoothing, threshold dependence and localisation in cluster inference. *Neuroimage* 2009; 44: 83–98.

44. D'Agostino RB and Stephens M. Tests for normal distribution in goodness-of-fit techniques. New York: Marcel Dekker, 1986
45. Blockley NP, Driver ID, Francis ST, et al. An improved method for acquiring cerebrovascular reactivity maps. *Magn Reson Med* 2011; 65: 1278–1286.
46. Bright MG, Bulte DP, Jezzard P, et al. Characterization of regional heterogeneity in cerebrovascular reactivity dynamics using novel hypocapnia task and BOLD fMRI. *Neuroimage* 2009; 48: 166–175.
47. Chan S-T, Evans KC, Song T-Y, et al. Cerebrovascular reactivity assessment with O₂-CO₂ exchange ratio under brief breath hold challenge. *PLoS One* 2020; 15: e0225915.
48. Kastrup A, Krüger G, Neumann-Haefelin T, et al. Assessment of cerebrovascular reactivity with functional magnetic resonance imaging: comparison of CO₂(2) and breath holding. *Magn Reson Imaging* 2001; 19: 13–20.
49. Prakash K, Chandran DS, Khadgawat R, et al. Correction for blood pressure improves correlation between cerebrovascular reactivity assessed by breath holding and 6% CO₂ breathing. *J Stroke Cerebrovasc Dis* 2014; 23: 630–635.
50. Jorge J, Figueiredo P, van der Zwaag W, et al. Signal fluctuations in fMRI data acquired with 2D-EPI and 3D-EPI at 7 tesla. *Magn Reson Imaging* 2013; 31: 212–220.
51. Chen K, Yang H, Zhang H, et al. Altered cerebrovascular reactivity due to respiratory rate and breath holding: a BOLD-fMRI study on healthy adults. *Brain Struct Funct* 2021; 226: 1229–1239.
52. Thrippleton MJ, Shi Y, Blair G, et al. Cerebrovascular reactivity measurement in cerebral small vessel disease: rationale and reproducibility of a protocol for MRI acquisition and image processing. *Int J Stroke* 2018; 13: 195–206.
53. DuBose LE, Weng TB, Pierce GL, et al. Association between cardiorespiratory fitness and cerebrovascular reactivity to a breath-hold stimulus in older adults: influence of aerobic exercise training. *J Appl Physiol (1985)* 2022; 132: 1468–1479.
54. Ivankovic M, Radman M, Gverovic-Antunica A, et al. Influence of hypertension and type 2 diabetes mellitus on cerebrovascular reactivity in diabetics with retinopathy. *Ann Saudi Med* 2013; 33: 130–133.
55. Atwi S, Shao H, Crane DE, et al. BOLD-based cerebrovascular reactivity vascular transfer function isolates amplitude and timing responses to better characterize cerebral small vessel disease. *NMR Biomed* 2019; 32: e4064.
56. Yazdani N, Kindy MS and Taheri S. CBF regulation in hypertension and Alzheimer's disease. *Clin Exp Hypertens* 2020; 42: 622–639.
57. Li Y, Li R, Liu M, et al. MRI study of cerebral blood flow, vascular reactivity, and vascular coupling in systemic hypertension. *Brain Res* 2021; 1753: 147224.
58. Harvey A, Montezano AC and Touyz RM. Vascular biology of ageing-implications in hypertension. *J Mol Cell Cardiol* 2015; 83: 112–121.
59. Petrica L, Petrica M, Vlad A, et al. Cerebrovascular reactivity is impaired in patients with non-insulin-dependent diabetes mellitus and microangiopathy. *Wien Klin Wochenschr* 2007; 119: 365–371.
60. Kadoi Y, Hinohara H, Kunimoto F, et al. Diabetic patients have an impaired cerebral vasodilatory response to hypercapnia under propofol anesthesia. *Stroke* 2003; 34: 2399–2403.
61. Tomoto T, Tarumi T and Zhang R. Central arterial stiffness, brain white matter hyperintensity and total brain volume across the adult lifespan. *J Hypertens* 2023; 41: 819–829.
62. Jefferson AL, Cambronero FE, Liu D, et al. Higher aortic stiffness is related to lower cerebral blood flow and preserved cerebrovascular reactivity in older adults. *Circulation* 2018; 138: 1951–1962.
63. Hussein A, Matthews JL, Syme C, et al. The association between resting-state functional magnetic resonance imaging and aortic pulse-wave velocity in healthy adults. *Hum Brain Mapp* 2020; 41: 2121–2135.
64. Hajjar I, Marmorelis V, Shin DC, et al. Assessment of cerebrovascular reactivity during resting state breathing and its correlation with cognitive function in hypertension. *Cerebrovasc Dis* 2014; 38: 10–16.
65. Webb AJS and Werring DJ. New insights into cerebrovascular pathophysiology and hypertension. *Stroke* 2022; 53: 1054–1064.
66. Feener EP and King GL. Vascular dysfunction in diabetes mellitus. *Lancet* 1997; 350 Suppl 1: SI9–13.
67. Giordani I, Di Flaviani A, Picconi F, et al. Acute hyperglycemia reduces cerebrovascular reactivity: the role of glycemic variability. *J Clin Endocrinol Metab* 2014; 99: 2854–2860.
68. Jansen JFA, van Bussel FCG, van de Haar HJ, et al. Cerebral blood flow, blood supply, and cognition in type 2 diabetes mellitus. *Sci Rep* 2016; 6: 10–19.
69. An Y, Kang Y, Lee J, et al. Blood flow characteristics of diabetic patients with complications detected by optical measurement. *Biomed Eng Online* 2018; 17: 25.
70. Petrica L, Vlad A, Gluhovschi G, et al. Proximal tubule dysfunction is associated with podocyte damage biomarkers nephrin and vascular endothelial growth factor in type 2 diabetes mellitus patients: a cross-sectional study. *PLoS One* 2014; 9: e112538.
71. Zhen YF, Zhang J, Liu XY, et al. Low BDNF is associated with cognitive deficits in patients with type 2 diabetes. *Psychopharmacology (Berl)* 2013; 227: 93–100.
72. Raichle ME, MacLeod AM, Snyder AZ, et al. A default mode of brain function. *Proc Natl Acad Sci U S A* 2001; 98: 676–682.
73. Chen JJ, Rosas HD and Salat DH. Age-associated reductions in cerebral blood flow are independent from regional atrophy. *Neuroimage* 2011; 55: 468–478.
74. Donahue MJ, Strother MK, Lindsey KP, et al. Time delay processing of hypercapnic fMRI allows quantitative parameterization of cerebrovascular reactivity and blood flow delays. *J Cereb Blood Flow Metab* 2015; 36: 1767–1779.

75. Leung J, Duffin J, Fisher JA, et al. MRI-based cerebrovascular reactivity using transfer function analysis reveals temporal group differences between patients with sickle cell disease and healthy controls. *Neuroimage Clin* 2016; 12: 624–630.
76. Sam K, Peltenburg B, Conklin J, et al. Cerebrovascular reactivity and white matter integrity. *Neurology* 2016; 87: 2333–2339.
77. Stickland RC, Zvolanek KM, Moia S, et al. A practical modification to a resting state fMRI protocol for improved characterization of cerebrovascular function. *Neuroimage* 2021; 239: 118306.
78. Thomas BP, Liu P, Park DC, et al. Cerebrovascular reactivity in the brain white matter: magnitude, temporal characteristics, and age effects. *J Cereb Blood Flow Metab* 2014; 34: 242–247.
79. Holmes KR, Tang-Wai D, Sam K, et al. Slowed temporal and parietal cerebrovascular response in patients with Alzheimer's disease. *Can J Neurol Sci* 2020; 47: 366–373.
80. Tong Y and Frederick BD. Tracking cerebral blood flow in BOLD fMRI using recursively generated regressors. *Hum Brain Mapp* 2014; 35: 5471–5485.
81. Tong Y, Yao JF, Chen JJ, et al. The resting-state fMRI arterial signal predicts differential blood transit time through the brain. *J. Cereb Blood Flow Metab* 2018; 271678X17753329
82. Christen T, Jahanian H, Ni WW, et al. Noncontrast mapping of arterial delay and functional connectivity using resting-state functional MRI: a study in moyamoya patients. *J Magn Reson Imaging* 2015; 41: 424–430.
83. Mitra A, Snyder AZ, Hacker CD, et al. Lag structure in resting-state fMRI. *J Neurophysiol* 2014; 111: 2374–2391.
84. Amemiya S, Takao H and Abe O. Origin of the time lag phenomenon and the global signal in resting-state fMRI. *Front Neurosci* 2020; 14: 596084.
85. Yao JF, Yang H-CS, Wang JH, et al. A novel method of quantifying hemodynamic delays to improve hemodynamic response, and CVR estimates in CO2 challenge fMRI. *J Cereb Blood Flow Metab* 2021; 41: 1886–1898.
86. Zvolanek KM, Moia S, Dean JN, et al. Comparing end-tidal CO₂, respiration volume per time (RVT), and average gray matter signal for mapping cerebrovascular reactivity amplitude and delay with breath-hold task BOLD fMRI. *Neuroimage* 2023; 272: 120038.
87. Gong J, Stickland RC and Bright MG. Hemodynamic timing in resting-state and breathing-task BOLD fMRI. *NeuroImage* 2023; 274: 120120.
88. Aso T, Jiang G, Urayama S-I, et al. A resilient, non-neuronal source of the spatiotemporal lag structure detected by BOLD signal-based blood flow tracking. *Front Neurosci* 2017; 11: 256.
89. Thomas BP, Liu P, Aslan S, et al. Physiologic underpinnings of negative BOLD cerebrovascular reactivity in brain ventricles. *Neuroimage* 2013; 83: 505–512.
90. Gallichan D and Jezzard P. Modeling the effects of dispersion and pulsatility of blood flow in pulsed arterial spin labeling. *Magn Reson Med* 2008; 60: 53–63.
91. Rendell M, Bergman T, O'Donnell G, et al. Microvascular blood flow, volume, and velocity measured by laser doppler techniques in IDDM. *Diabetes* 1989; 38: 819–824.
92. Novak V, Last D, Alsop DC, et al. Cerebral blood flow velocity and periventricular white matter hyperintensities in type 2 diabetes. *Diabetes Care* 2006; 29: 1529–1534.
93. Kermani P and Hempstead B. BDNF actions in the cardiovascular system: roles in development, adulthood and response to injury. *Front Physiol* 2019; 10: 455.
94. Peng S-L, Chen X, Li Y, et al. Age-related changes in cerebrovascular reactivity and their relationship to cognition: a four-year longitudinal study. *Neuroimage* 2018; 174: 257–262.
95. Perret RS and Sloop GD. Increased peak blood velocity in association with elevated blood pressure. *Ultrasound Med Biol* 2000; 26: 1387–1391.